nature physics

ARTICLES

PUBLISHED ONLINE: 31 MAY 2009 | DOI: 10.1038/NPHYS1300

Experimental onset threshold and magnetic pressure pile-up for 3D reconnection

T. P. Intrator[1]*, X. Sun[1], G. Lapenta[2], L. Dorf[1] and I. Furno[3]

Magnetic reconnection changes the topology of magnetic field lines to a lower-energy state. This process can liberate stored magnetic field energy and accelerate particles during unsteady, explosive events. This is one of the most important processes in astrophysical, space and laboratory plasmas. The abrupt onset and cessation has been a long-standing puzzle. We show the first three-dimensional (3D) laboratory example of the onset and stagnation of magnetic reconnection between magnetized and parallel current channels (flux ropes) driven by magnetohydrodynamic (MHD) attraction and a 3D plasma-current-driven instability. Antiparallel magnetic field lines carried by these colliding flux ropes annihilate and drive an electric field. The inflow soon exceeds a threshold for the formation of a reconnection current layer. Magnetic flux and pressure pile up just outside this layer, and eventually become large enough to support MHD back-reaction forces that stall the inflow and stagnate the reconnection process.

For more than half a century it has been realized that a class of processes known variously as magnetic merging, magnetic field annihilation or magnetic reconnection must be the key to global changes in magnetic topology in cosmic solar, magnetosphere and laboratory plasma environments. Energy stored in stressed magnetic fields can produce large-scale explosive events that spontaneously evolve owing to unsteady and impulsive local processes in small volumes of space, and energize particles. For many physical systems of interest, reconnection does not start or proceed in a steady manner, but rather there are unsteady periods of time during which magnetic flux is accumulated, followed by rapid energy dissipation events. This situation is inherently three dimensional (3D).

It has become increasingly apparent that magnetic reconnection[1,2] is important in heliosphere[3], astrophysical[4] and laboratory[5,6] plasmas. The classic and physically appealing picture of reconnection is the 2D Sweet–Parker[7,8] type. Plasma that is a nearly perfect electrical conductor entrains antiparallel magnetic fields. Two mutually approaching, steady flows in the reconnection plane advect these antiparallel magnetic fields as they collide. An X point forms in the region of closest approach of the magnetic field lines, magnetohydrodynamics (MHD) is locally violated and according to Ampere's law the jump in magnetic field induces an out-of-plane reconnection current in a diffusion region. Reconnection could occur at any or all locations on a line in the out-of-plane direction, which includes the X point(s).

Recent satellite[9] and laboratory[10] data demonstrate that many situations are 3D. The mutual approach and merging of two or more flux ropes represents the simplest model. Flux ropes[11–13] are plasma 'wires' or current channels that can relax (twist, kink and so on) and approximately align with a helically serpentine magnetic field. Reconnection events are often impulsive[14,15], although there is some evidence for quasi-steady-state reconnection in a current sheet between the Sun and the Earth[16]. Flux ropes can attract each other and merge at a 3D patch, and then sporadic dynamics become an important consideration.

Tremendous efforts have focused on the reconnection rate, usually modelled with asymptotic magnetic fields embedded in steady flows. However, little is known regarding the fundamental question: what causes the onset and termination of reconnection?

Plasma 'wires' with mass respond to MHD forces in 3D

The long experimental history includes toroidal experiments that have created 2D (ref. 6) reconnection geometries, along with some 'spontaneous'[17] reconnection events. 3D reconnection scenarios[18] have been identified in linear geometries[10,19]. All of these experiments program their magnetic time history and initial conditions using magnet coils that determine the magnetic drive and location of the X line. However, internal forces during magnetic self-organization are important for large-scale systems[20]. Here, we show a laboratory example of 3D magnetic reconnection where current-carrying 'wires' that create the magnetic geometry are composed of plasma flux ropes with mass and inertia, are subject to Newton's law dynamics and can relax in 3D. Reconnection is impulsively initiated between two freely moving parallel current flux ropes that attract each other, forcing together the oppositely directed magnetic fields between them. As the current in each flux rope ramps up, so does the azimuthal magnetic field surrounding each current channel, and therefore the original background axial magnetic field becomes helical. 3D kink instabilities[12,13] grow, which reflects the tendency of flux ropes to align helically with the net magnetic field. Each flux-rope collision and flux annihilation region becomes a 3D patch of reconnection.

Overview of experimental findings

Experimentally, we start with a twin flux rope and magnetic island structure[21,22]. We show a slow inflow threshold for the flux annihilation speed, beyond which there is acceleration culminating in a pile-up of magnetic flux accompanied by a change in the magnetic topology to a merged reconnected geometry. We then argue that the magnetic field $\mathbf{B}$ that piles up just outside the reconnection diffusion region interacts with the current density $\mathbf{J}$ and gives rise to $\mathbf{J} \times \mathbf{B}$ forces that push back on the merging flux ropes and stagnate the reconnection process. Even though the plasma is moderately collisional, we believe this is a general result because (1) we can distinguish between resistive diffusion

[1]Los Alamos National Laboratory, P-24 Plasma Physics, Los Alamos, New Mexico 87545, USA, [2]Centre for Plasma Astrophysics, Katholieke Universiteit Leuven, BE-3001, Belgium, [3]CRPP-EPFL, Bâtiment PPB, 1015 Lausanne, Switzerland. *e-mail: intrator@lanl.gov.

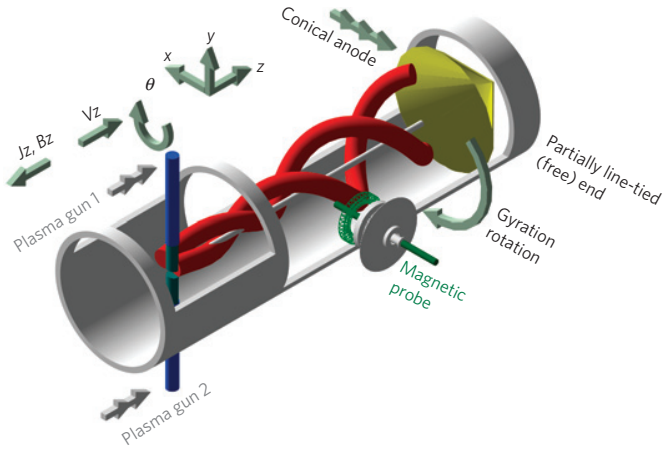

Figure 1 | Schematic diagram of the RSX experiment. The diagram shows the coordinate system and geometry (single arrows), two plasma guns (double arrows) that are inserted radially but create axial flux ropes, two kinking flux ropes, an external conical anode (triple arrow) that enables adjustment of the axial boundary condition, a fiducial line (fictitious and only for reference) at the vessel **z** axis and a magnetic probe inserted through a 3D probe positioner. The radial width is exaggerated by a factor of 4.

and anomalously fast flux annihilation and (2) simulations carried out over a range of Lundquist numbers including our experimental values show similar results.

Experiment

A schematic diagram of the reconnection scaling experiment[23] (RSX) is shown in Fig. 1, where we have exaggerated the radial scale and field line pitch by a factor of 4 to highlight the plasma structure. Two plasma guns generate two hydrogen plasma current channels, embedded in a background magnetic guide field $\mathbf{B}_{z0} = 100$ gauss. Each column has a current distribution radius $a \sim 2$–3 cm, with an azimuthal magnetic field that vanishes on its axis and radially extends twice this far. The axial boundary condition is an external anode located $L_z \approx 96$ cm from the plasma gun[24]. The guns are fired at time $t = 0$ and are biased negatively to extract a plasma current $I_p < 0$ from the gun plasma source. The diameter distance between the two plasma guns is $L_\perp \sim 6$ cm.

Each flux-rope plasma current $I_p(t)$ ramps up during the time interval 1.200–1.220 ms for which we show reconnection data. In addition to the mutual attraction of the flux ropes, the kink instability[13] drives each column into two gyrating helices[25] that collide to create 3D merging regions of patchy reconnection, verified by measurements at several nearby axial positions. Meanwhile the current density $\mathbf{J}_z(x, y)$ and magnetic field $\mathbf{B}_\perp = \mathbf{B}_{xy}(x, y)$ distributions evolve as the flux ropes attract each other.

The current channels are emitted from a current source with large impedance relative to the plasma[13]. Rather than following a programmed coil voltage drive, the plasma chooses its own steady voltage bias that is small and time independent. A steady electrostatic axial electric field $\mathbf{E}_{z,es} \approx -1\,\mathrm{V\,m^{-1}}$ ($\pm 20\%$) < 0 drives the two flux ropes[13]. The flux rope-to-rope attraction force and velocity can be experimentally increased by increasing the flux-rope currents I_p and/or decreasing the background guide magnetic field, which decreases the magnetic compressibility and the field-line-tension restoring force.

As shown in Fig. 1, a magnetic probe with multiple (x–y or x–z) coil pairs spaced at 5 mm intervals is placed at $\theta = 180°$, $z = 48$ cm from the gun in a 3D probe positioner[26] to carry out a magnetic field profile scan in the x–y cutplane. A triple probe at $\theta = 0°$, $z = 48$ cm is used to measure the plasma density, pressure and potential profiles[24] for the flux rope and background plasma. The flux-rope density is much greater than the background plasma. Experimental shots are reproducible until the end of the reconnection phase, with many collated shots per data set.

Similar to the reconnection occurring in nature, the merging of flux ropes in RSX is 3D and represents co-helicity, impulsively reconnecting field lines at a small oblique half angle. As this angle is small and the axial gradient lengths are large compared with the perpendicular gradient lengths, the magnetic flux contours in the 2D x–y cutplane still exhibit recognizable 2D coalescing magnetic island geometry. The finite length and non-periodic axial boundary conditions distinguish the RSX reconnection geometry from other toroidal experiments and periodic simulations because (1) axial structure can be important and (2) the particles neither recirculate periodically nor are constrained to remain near any 2D reconnection plane.

Reconnection data

The current density $\mathbf{J}_z(x, y)$ derived from magnetic field $\mathbf{B}_\perp < 10$ gauss data showing reconnection is shown in Fig. 2. The measured vector magnitude and direction of $\mathbf{B}_x$ and $\mathbf{B}_y$ were used to calculate out-of-plane current density contours $\mu_0 \mathbf{J}_z(x, y; t) = \nabla \times \mathbf{B}_\perp$. Figure 2a shows two initial flux ropes almost vertically aligned with $\mathbf{J}_z < 0$. Figure 2b shows that the two flux tubes have rotated clockwise about their centre of mass, owing to the kink motion of individual flux ropes. Triple probe measurements (not shown here) of plasma density, temperature and pressure confirm this rotation. Here, each flux rope is fixed at the gun and partially line tied at the other end[12,27]. Figure 2c shows $\mathbf{J}_z$ contours when the flux annihilation rate rises from zero. Figure 2d shows the development of a reconnection region with a reversed current $\mathbf{J}_z > 0$ and changed magnetic topology.

There is a distorted $\mathbf{J}_z < 0$ region that contains the remnants of the original two flux ropes surrounding a $\mathbf{J}_z > 0$ reconnection region. Reversed currents also exist at the top and bottom in Fig. 2c–e. Simulations of RSX (see Fig. 19 in ref. 28) suggest that this is due to kink motion of separate field lines within each flux rope. Figure 2e shows the well-developed reconnection geometry when the reconnection rate is maximum. Vector $\mathbf{B}_\perp$ arrows are overlaid in Fig. 2a,b,f.

Line cut across reconnection region

As shown in Fig. 3a, the initial magnetic field between the flux ropes is very small. Later in time, the flux-rope currents gradually ramp up by 50%, but the magnetic field in Fig. 3b increases by a very large factor from a fraction of a gauss to roughly 5 gauss. Magnetic flux from transverse $\mathbf{B}_\perp(s)$ piles up as magnetic reconnection develops between $t = 1.200$ and 1.221 ms. The measured reconnection current $\mathbf{J}_z > 0$ (sign reversed from flux-rope current) corresponds to an electron diffusion region with radial width > 0.4 cm, which is three times larger than the electron skin depth $c/\omega_{pe} \approx 0.15$ cm.

Generalized Ohm's law

Customarily one estimates the reconnection rate and electric field from the time derivative of the vector potential. However, as the pile-up of magnetic flux and pressure (stagnation) obscure the interpretation of time derivatives, a lower limit is calculated instead. We define the boundary of the reconnection region in the x–y cutplane to be the contour where the current density $\mathbf{J}_z(t)$ changes sign from the $\mathbf{J}_z < 0$ flux-rope drive to $\mathbf{J}_z > 0$ induced reconnection current. To estimate the axial electric field before and during reconnection, a generalized two-fluid and spatial scale Ohm's law[2] is useful. We evaluate a cutplane average over the reconnection current region. The terms on the right hand side of equation (1) include: (1) anomalous resistivity $\eta_\parallel^*$ that is expected to be at least as large as the Spitzer value $\eta_\parallel$, (2) the electron inertia term total

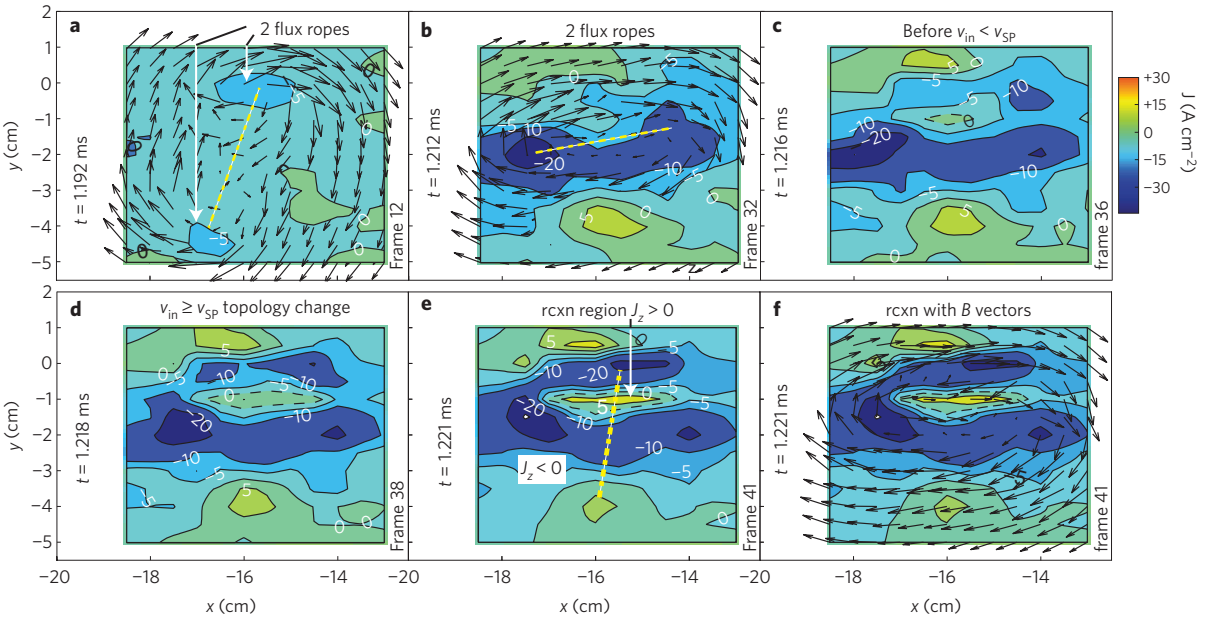

Figure 2 | Current density $J_z(x,y)$ derived from magnetic $B_\perp$ data for $B_{z0} = 100$ gauss in the x–y cutplane at $z = 48$ cm. The panels show contours of calculated $\mathbf{J}_z = \nabla \times \mathbf{B}_\perp/\mu_0$, also corresponding to flux contours. **a**, At $t = 1.192$ ms, the two flux ropes start out vertically aligned. **b**, At $t = 1.212$ ms, the cross-section line s has rotated clockwise. **c**, At $t = 1.216$ ms, v_{in} and the flux annihilation rate rise. **d**, At $t = 1.218$ ms, v_{in} exceeds v_{SP} and the magnetic topology changes from two flux ropes to a $J_z < 0$ region surrounding a $J_z > 0$ reconnection region (dashed zero contours). **e**, At $t = 1.221$ ms, the reconnection (rcxn) rate is maximum; the dashed line indicates a cut across the reconnection layer. **f**, $\mathbf{B}_\perp$ arrow vectors overlaid on $J_z(x,y)$ contours.

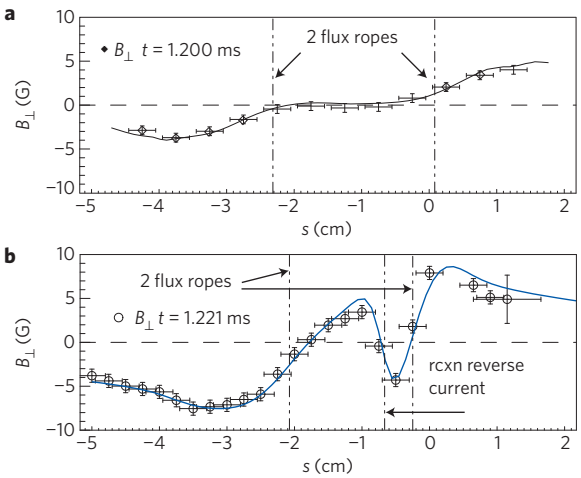

Figure 3 | Magnetic field evaluated on a line s that crosses the interaction region between the two colliding flux ropes. Before ($t = 1.200$ ms) (**a**) and during ($t = 1.221$ ms) (**b**) reconnection where there is field pile-up around the reconnection reversed-current region. The curve fits derive from the current density $J_z(s)$ with Bennett pinch profiles. The error bars indicate the time-averaging period and the measurement uncertainty, and data scatter due to averaging several shots per location.

time derivative of the current density $\mathbf{J}_z$, (3) the Hall $\mathbf{J} \times \mathbf{B}$ term and (4) divergence of the electron pressure tensor $\mathbf{P}_e (e > 0)$

$$\mathbf{E}_{z,\mathrm{tot}} + \mathbf{v}_{\mathrm{in}} \times \mathbf{B} = \eta_\parallel^* \mathbf{J}_z + \mu_0 (c^2/\omega_{\mathrm{pe}}^2)[\partial/\partial t(\mathbf{J}_z) + \nabla \cdot (\mathbf{v}\mathbf{J} + \mathbf{J}\mathbf{v})] + \mathbf{J} \times \mathbf{B}/en - \nabla \cdot \mathbf{P}_e/en \quad (1)$$

Using the geometry of Fig. 2e, we compare each term to $\mathbf{v}_{\mathrm{in}} \times \mathbf{B}$ to show that anomalous resistivity $\eta_\parallel^*$ dominates in the electron diffusion region. The diffusion region is larger than the electron skin depth maximum scale size for electron inertia effects[2,29]. The Hall term includes products $\mathbf{J}_x \times \mathbf{B}_y$ and $\mathbf{J}_y \times \mathbf{B}_x$ associated with ion skin depth c/ω_{pi} length scales, where c is the speed of light and ω_{pi} is the ion plasma frequency. These are small near the $\mathbf{J}_z > 0$ reconnection current layer where the magnetic field $\mathbf{B}_\perp$ vanishes. The last term contains derivatives $\partial \mathbf{P}_{zx}/\partial x + \partial \mathbf{P}_{yz}/\partial y$ of the electron pressure tensor off-diagonal elements. These are important on the hybrid spatial scale of the electron meandering orbit[30,31] $\lambda_y = (r_{\mathrm{Ge}\perp} B_x/B_x')^{1/2}$. We evaluate the electron gyro radius $r_{\mathrm{Ge}\perp}$ and scalar magnetic scale length B_x/B_x' where $B_x' = \partial B_x/\partial y$, at the edge of the diffusion region. Our experimental $B_{z0} = 100$ gauss is 10 times larger than necessary to magnetize the meander orbits and reduce the pressure tensor terms. A large guide field $B_{z0} \geq B_x'\ \lambda_y$ exceeds that of the reconnecting field B_x at the furthest excursion of the bounce motion. For the RSX data in Fig. 3b, $B_x/B_x' \approx 0.4$ cm, $r_{\mathrm{Ge}\perp} \approx 1.2$ cm, $\partial B_x/\partial y \approx 13$–$14$ gauss cm^{-1}, $\lambda_y \approx 0.7$ cm and $B_x'\lambda_y \approx 10$ gauss.

Estimation of the axial electric field

Using Spitzer resistivity ($\eta_\parallel$), we recast equation (1) as the inequality

$$\mathbf{E}_{z,\mathrm{tot}} = \mathbf{E}_{z,\mathrm{ind}} + \mathbf{E}_{z,\mathrm{es}} > \eta_\parallel \mathbf{J}_z - \mathbf{v} \times \mathbf{B} \quad (2)$$

where the total axial electric field is $\mathbf{E}_{z,\mathrm{tot}} = \mathbf{E}_{z,\mathrm{ind}} + \mathbf{E}_{z,\mathrm{es}}$. Electrostatic, time-independent $\mathbf{E}_{z,\mathrm{es}} < 0$ is measured with a swept Langmuir probe and does not contribute to the inductive reconnection field. Before reconnection, the inductive field $\mathbf{E}_{z,\mathrm{ind}} = -\mathrm{d}\mathbf{A}_z/\mathrm{d}t$ is obtained from solutions to a Poisson equation

$$\nabla^2 \mathbf{A}_z = \mu_0 \mathbf{J}_z = -\nabla \times \mathbf{B}_\perp \quad (3)$$

where the vector potential is $\mathbf{A} + \nabla\chi$ with the gauge $\nabla\chi = -\int E_{z,\mathrm{es}}\,\mathrm{d}t$, from the magnetic data $\mathbf{B}_\perp$ in Fig. 2a–d. The boundary conditions require that $\mathbf{B}_\perp$ and $\mathbf{A}_z$ vanish for large $|x|$, $|y| > 12$ cm from the flux ropes.

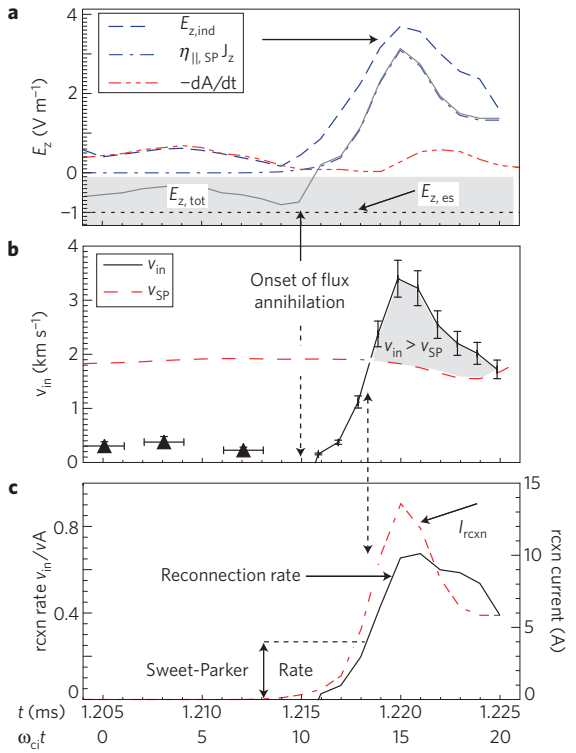

Figure 4 | Reconnection onset threshold and rate. a, The estimated lower bound for the electric field showing the time history of total $E_{z,tot}$, inductive $E_{z,ind}$ measured from the time-changing flux before stagnation and the $\eta_\parallel J_z$ contribution after reconnection is underway, and slowly varying electrostatic $E_{z,es}$, which supports the flux-rope current. Flux annihilation commences before the sign of $E_{z,tot}$ changes at $t = 1.215$ ms, when the $E_{z,tot}$ field starts to rise. **b**, The approach speed of the two flux ropes calculated from the flux contours in Fig. 2 (triangles) for early time, and $E_z/B_\perp$ from equation (2) (solid line) for times after 1.215 ms, compared with the Sweet–Parker speed. The error bars correspond to the averaging time and uncertainty in $B_\perp$ data and calculated J_z. The shaded region corresponds to the time period $t > 1.218$ ms, where $v_{in} \geq v_{SP}$. **c**, Reconnection rate and reconnection reversed current I_p, which is an integral measure of the magnetic field line integral around the reconnection region, corresponding to topology change and flux pile-up.

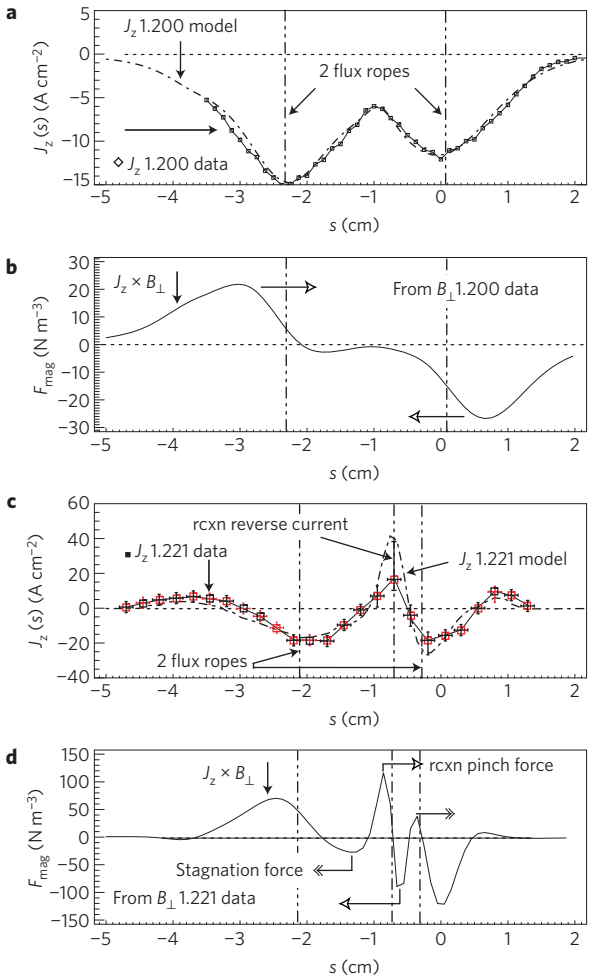

Figure 5 | J × B forces stagnate reconnection process. a, Current density computed from $\nabla_\perp \times B_\perp$, where $B_\perp$ in the x–y plane is perpendicular to line s, overlaid with the pinch model $J_z(s)$ at time $t = 1.200$ ms (before reconnection). The vertical dash–dot–dot lines indicate the fit locations for the flux-rope centroids. **b**, The $J_z \times B_\perp$ force densities at $t = 1.200$ ms before reconnection, where the hollow-head arrows indicate the attraction force. **c**, $J_z(s)$ computed from B data overlaid with the pinch model $J_z(s)$ at time $t = 1.221$ ms (during reconnection). The vertical dash–dot–dot lines now show three magnetic axes. **d**, Hollow-head arrows indicate a pinch force density inside the reconnecting flux rope at $y = -0.6$ to -0.8 cm, and double-head arrows show a repelling $J_z \times B_\perp$ back-reaction force density exerted by the reconnection region on the incoming flux ropes at $s = -1.5$ cm, -0.3 cm.

However, evaluation of the laboratory-frame time derivative during reconnection is not straightforward because it is small and stagnating[32] at the edge of the reconnection region. This is because flux is lost as fast as it is piling in: to annihilation, outward diffusion and expulsion of reconnected flux. The total time derivative $\mathrm{d}/\mathrm{d}t = \partial/\partial t + \mathbf{v}_s \cdot \nabla_s$ includes a negative loss rate and a positive convective inflow, where the subscript s refers to the line connecting two flux-rope centroids (see Figs 2b and 3). The dash–dot–dot line in Fig. 4a shows that the experimental $\mathrm{d}\mathbf{A}_z(t)/\mathrm{d}t$ from equation (3) is small. This approach fails to estimate the substantial $\mathbf{E}_z$ that must exist in the laboratory frame during reconnection. Alternatively, we use equation (2) and experimental data from Fig. 2 averaged over the reconnection $\mathbf{J}_z > 0$ X-point region (where $v \times \mathbf{B}$ vanishes). Figure 4a also shows the lower-bound estimates for inductive $\mathbf{E}_{z,ind} = \eta_\parallel \mathbf{J}_z - \mathbf{E}_{z,es}$ (dashed line), and total $\mathbf{E}_{z,tot} \geq \eta_\parallel \mathbf{J}_z$ (solid line).

$\mathbf{E}_{z,tot}$ was used to estimate a lower bound for the $\mathbf{E}_z \times \mathbf{B}_\perp$ flux transport inflow speed at the edge of the reconnection region. Figure 4b shows the inflow speed (triangles) evaluated early in time using equivalent current density or flux contours along the line (Fig. 2a,b) labelled s, which rotates with time, and later in time using $\mathbf{v}_{in}(t) = \mathbf{E}_{z,tot} \times \mathbf{B}_\perp / \mathbf{B}_\perp^2$. Here, $\mathbf{B}_\perp$ in the x–y plane is evaluated perpendicular to line s.

Threshold for topology change and flux pile-up

Even though the flux is already being annihilated, flux pile-up theoretically initiates when the inflow speed v_{in} delivers flux faster than either resistive diffusion or flux annihilation can process it[4,21,33]. In this case, v_{in} must exceed the Sweet–Parker speed $v_{SP} = v_A/S^{1/2}$, where $v_A(t) = B_\perp(t)/(\mu_0 n(t) m_i)^{1/2}$ with $B_\perp$ and nm_i evaluated at the $\mathbf{J}_z > 0$ diffusion region edge, and the Lundquist number $S_\perp = \tau_{D\perp}/\tau_{A\perp}$ is the ratio of the resistive diffusion time to the Alfvén transit time. The reconnection flux annihilation rate estimated as v_{in}/v_A in Fig. 4c turns on at $t = 1.216$ ms, corresponding to the contours of $\mathbf{J}_z(x, y)$ in Fig. 2c. Several microseconds later at $t = 1.218$ ms, the flux inflow and annihilation rate in Fig. 3b,c have exceeded the Sweet–Parker values. Correspondingly, $\mathbf{J}_z(x, y)$ in Fig. 2d exhibits a change in current density (magnetic) topology. The flux pile-up starts when the $\mathbf{J}_z$ topology changes in Fig. 2d as v_{in}

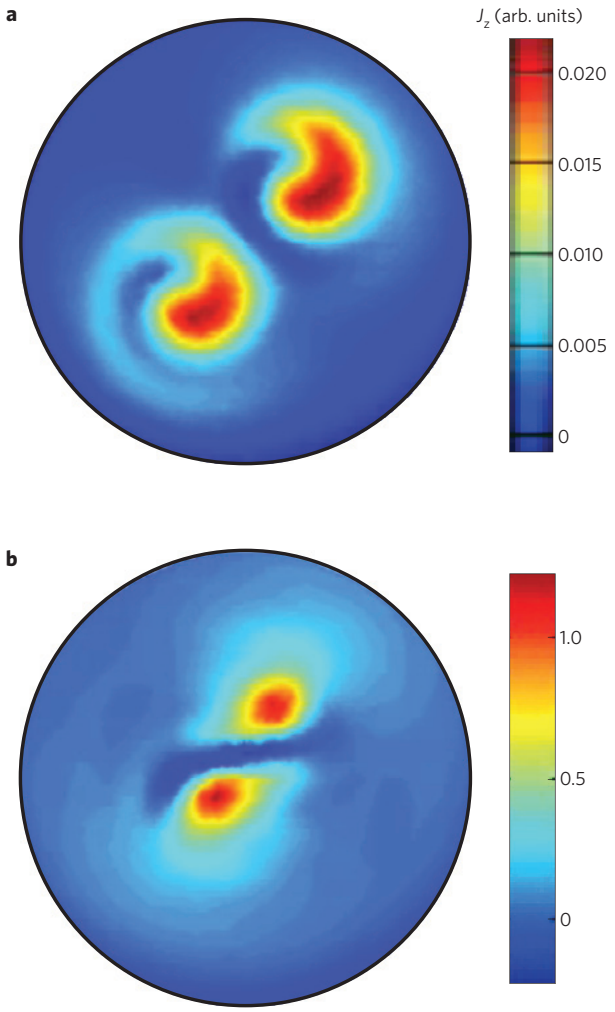

Figure 6 | Computer FLIP3D simulations using a visco-resistive MHD model and realistic boundary conditions of the two RSX flux ropes that mutually attract. a, Two flux ropes with $J_z > 0$ at $\omega_{ci}t = 7$ before reconnection. The curling flux-rope sections have some similarity to those of Fig. 2c,d. **b**, More intense J_z at later time $\omega_{ci}t = 42$, with an 'S'-shaped reconnection reversed current $J_z(x, y) < 0$ between the two $J_z > 0$ flux ropes.

exceeds v_{SP}, and several microseconds later is easily discerned in Fig. 3b. For a larger ratio of $B_z/B_\perp$, the inflow speed is slower ($v_{in} < v_{SP}$), no reconnection layer is formed and the two flux ropes bounce[34].

Stagnation of reconnection and flux pile-up

It is theoretically expected that the magnetic pressure will eventually slow down or stall the merging process[2,32,33,35]. Early in time, the flux-rope current data $\mathbf{J}_z(s)$ as shown in Fig. 5a give rise to $\mathbf{J}_z(s) \times \mathbf{B}_\perp(s)$ force densities that initially attract the flux ropes, as indicated by the hollow-head arrows in Fig. 5b. During reconnection, the reversed current $J_z(s)$ as shown in Fig. 5c and magnetic field pile-up give rise to $\mathbf{J}_z(s) \times \mathbf{B}_\perp(s)$ forces that repel the incoming flux ropes as shown in Fig. 5d. The double-head arrows indicate that the repulsive $\mathbf{J}_z(s) \times \mathbf{B}_\perp(s) \approx 30$–$40\ \mathrm{N\,m^{-3}}$, at locations $s = -1.5$, -0.3 cm, is sufficient to stagnate two approaching flux-rope momenta with our measured mass density and mutual inflow speed of 3–4 $\mathrm{km\,s^{-1}}$ estimated from Fig. 4b. As this repulsion force is at the outside edge of the current sheet, this conclusion is not affected by possible errors in the pinch current density curve fits to the data inside the reconnection region.

Comparison with computer simulation

The data in Fig. 2 are consistent with a fluid-implicit-particle simulation FLIP3D-MHD. Lagrangian particle interactions computed on a grid and viscous, resistive MHD flow equations[28,36] allow reconnection to proceed. The movie frames in Fig. 6a (before reconnection, $\omega_{ci}t = 7$) and Fig. 6b (during reconnection, $\omega_{ci}t = 42$) show similar results for a wide range of Lundquist numbers and system sizes that include the experimental RSX parameters shown here. The curled spiral-like flux-rope shapes in Fig. 6a resemble Fig. 2c,d, and the central reconnection region shape is reminiscent of a quasi-separatrix layer[2,37].

Summary

Magnetic reconnection, driven by instability (waves) and dynamics may couple in a natural way to other wave modes. It is thought that the fast collisionless reconnection rate is increased by dispersive waves with increased phase speed at large wavenumber or small spatial scales[38]. Whereas dispersive whistler and drift waves are predicted to be important for many experiments (for example, the magnetic reconnection experiment[6,10,39]), kinetic Alfvén waves[38] should also be relevant for RSX data.

Our data exhibit several experimental features not usually considered in 2D models. The guide field $B_{z0} = 100$ gauss is 10 times larger than $\mathbf{B}_\perp$. For a small enough background magnetic field (where $B_{z0} < 100$ gauss), the flux ropes merge and reconnect, but for larger B_{z0} they bounce. Angular momentum, which is usually a robust invariant, seems to be important when the two flux ropes orbit each other. These orbits could be an example of a Keplerian central force problem with a $\mathbf{J} \times \mathbf{B}$ attraction force that scales as $1/r$ and not gravitational $1/r^2$. Other features shown by Figs 3 and 5 are asymmetric reconnection fields and forces[40] on either side of the reconnection layer. This more likely represents the typical case in nature than ideal and symmetric configurations.

Methods

We describe here how we carried out the data analyses and the normalization of the reconnection time, rate and speed. RSX (ref. 23) coordinates as in Fig. 1 invoke an x–y reconnection ($\perp$) plane, where z is the direction of the reconnection current, which differs from solar magnetic coordinates where reconnection is discussed in the x–z plane and y is the out-of-plane direction. Two plasma guns are inserted radially and generate two axial hydrogen plasma current channels, embedded in a background magnetic guide field $\mathbf{B}_{z0}$. The distance between the two plasma flux ropes at the plasma guns is $L_\perp \sim 6$ cm. Electron temperature $T_e \approx 6$–14 eV, plasma density $n \approx 1$–$3 \times 10^{13}\ \mathrm{cm^{-3}}$, estimated plasma Spitzer resistivity due to Coulomb electron–ion collisions is $\eta_\perp \approx 20$–$25\ \mu\Omega$-m and $\eta_\parallel \approx 10$–$12\ \mu\Omega$-m. The mean free path for Coulomb electron–ion collisions using $\eta_\perp$ is approximately 10–20 cm $\gg L_\perp$. Each column has a radius corresponding to the current distribution width $a \sim 2$–3 cm, with a wider magnetic field distribution width, and is terminated at an external anode to length $L_z \approx 96$ cm (ref. 24). Although we measure a net sonic fluid flow with a Mach probe from the gun to the anode, we do not consider any axial flow effects on the reconnection. The ion and electron inertial lengths are respectively $c/\omega_{pi} \approx 4$–5 cm and $c/\omega_{pe} \approx 0.1$ cm, where ω_{pi}, ω_{pe} and c are respectively the ion and electron plasma frequencies and the speed of light. In the initial flux ropes, the plasma $\beta_{z0} \approx 30$–50% and the axial Alfvén speed referenced to the strong guide field $B_{z0} = 100$ gauss is $v_{Az} \approx 70\ \mathrm{km\,s^{-1}}$. $v_{A\perp} \approx 7$–$8\ \mathrm{km\,s^{-1}}$ referenced to the $\mathbf{B}_\perp \approx 10$ gauss reconnection field, leading to a Lundquist number $S_\perp = L_\perp v_{A\perp}/(\eta_\perp/\mu_0) = \tau_{D\perp}/\tau_{A\perp} \approx 15$–$20$. Here, $S_\perp$ is the ratio of resistive diffusion $\tau_{D\perp}$ to Alfvén transit $\tau_{A\perp}$ times in the perpendicular direction, and is used to gauge time and length scales.

Similar to the reconnection occurring in nature, the merging of flux ropes in RSX is 3D and represents impulsively reconnecting, co-helicity field lines at a small oblique half angle totalling approximately the flux-rope twist ($\approx 5°$) plus kink writhe ($\approx 0.7°$). In the 2D x–y cutplane picture of reconnection, information can be communicated between locations at the Alfvén speed $v_{A\perp}$, which also conveniently normalizes the reconnection rate. The Alfvén time is relevant even if ideal, uniform density, bulk waves are cut off. For example, a surface Alfvén wave spectrum exists for RSX parameters on the surface of a current-carrying column, which includes shear, kink and compressional modes[41].

Our data analyses take advantage of the analytic curve fits in Fig. 5 for the pinch-profile current density used by Anderson[2,32] to model time-dependent magnetic flux annihilation in a stagnation flow region. Model flux-rope currents' plus smaller induced return currents'[34] pinch profiles were used. These fits were

matched to $\mathbf{J}_z(s)$ data[24], where $J_z(s) = J_{0z}(1+x^2)^{-2}$, $x = (s-s_0)/a$, s_0 is the flux-rope magnetic axis and $J_z(a)/J_{0z} = 1/4$.

Typically the reconnection rate driven by the electric field $\mathbf{E}_{z,\mathrm{tot}}$ is normalized to the inflow speed $\mathbf{v}_{\mathrm{in}} = \mathbf{E}_{z,\mathrm{tot}} \times \mathbf{B}_\perp / \mathbf{B}_\perp^2$. The total electric field is $\mathbf{E}_{\mathrm{tot}} = -\nabla\phi_{\mathrm{p}} - \partial\mathbf{A}/\partial t$, where ϕ_{p} is the electrostatic scalar potential and $\mathbf{A}$ is the vector potential. We measure ϕ_{p} with a swept Langmuir probe. It supports a small background, steady-state, electrostatic (on the millisecond timescale) $\mathbf{E}_{z,\mathrm{es}} = -\nabla\phi_{\mathrm{p}}$ field that sustains each flux rope (Fig. 4a). The inductive reconnection electric field $\mathbf{E}_{z,\mathrm{ind}}$ is opposite in direction to and overcomes $\mathbf{E}_{z,\mathrm{es}}$.

During fast collisionless reconnection, dispersive waves with phase speed proportional to the wavenumber $\mathbf{k}$ (ref. 38) are thought to affect the reconnection outflow geometry and increase the reconnection rate at small scales. Assuming initial $\mathbf{B} = \mathbf{B}_x + \mathbf{B}_{z0}$, growth of $\mathbf{B}_y \approx \mathbf{B}_x$ during reconnection and $\mathbf{k} = \mathbf{k}_y$, two key dimensionless parameters are the ratio of plasma to magnetic pressure β_{k} outside the current sheet referenced to $\mathbf{B}_y$ and $\mu_x = (m_{\mathrm{e}}/m_{\mathrm{i}})(B^2/B_{\mathrm{k}}^2 + \beta_{\mathrm{k}}/2) \approx (m_{\mathrm{e}}/m_{\mathrm{i}})(1 + \beta_{z0}/\beta_{\mathrm{k}} + \beta_{\mathrm{k}}/2)$. These follow from three spatial scales, $\mathrm{d_s} = \mathrm{d_i}(1 + v_{\mathrm{A}}^2/c_{\mathrm{S}}^2)^{-1/2}$, $\mathrm{d_e} = c/\omega_{\mathrm{pe}}$ (which is the electron skin depth) and $\mathrm{d_k} = \mathrm{d_i}(\mathbf{B}^2/\mathbf{B}_{\mathrm{k}}^2 + c_{\mathrm{S}}^2/v_{\mathrm{Ak}}^2)^{-1/2}$, where c_{S} is the ion acoustic sound speed, $\mathrm{d_i} = c/\omega_{\mathrm{pi}}$ is the ion skin depth and $v_{\mathrm{A}} = \mathbf{B}^2/(\mu_0 n m_{\mathrm{i}})^{1/2}$ includes all of the $\mathbf{B}$ components. In this RSX experimental regime, $\mathrm{d_i} \approx 5$ cm, $\mathrm{d_e} \approx 0.17$ cm, $\mathrm{d_s} \approx 0.8$ cm and $\mathrm{d_k} \approx 0.5\,\mathrm{cm} \approx$ diffusion layer size, leading to $\beta_{\mathrm{k}} \approx 40 \gg 1$, $\beta_{z0} \approx 0.4$ and $\mu_x \approx 0.06 \ll 1$. Figure 2 in Rogers *et al.*[38] predicts both whistler and kinetic Alfvén wave effects during the reconnection process.

Received 9 October 2008; accepted 28 April 2009; published online 31 May 2009

References

1. Biskamp, D. *Magnetic Reconnection in Plasmas* (Cambridge Univ. Press, 2000).
2. Priest, E. R. & Forbes, T. *Magnetic Reconnection* (Cambridge Univ. Press, 2000).
3. Mozer, F. S., Phan, T. D. & Bale, S. D. The complex structure of the reconnecting magnetopause. *Phys. Plasmas* **10**, 2480–2485 (2003).
4. Kulsrud, R. M. *Plasma Physics for Astrophysics* (Princeton Univ. Press, 2005).
5. Taylor, J. B. Relaxation and magnetic reconnection in plasmas. *Rev. Mod. Phys.* **58**, 741–763 (1986).
6. Yamada, M. Review of controlled laboratory experiments on physics of magnetic reconnection. *J. Geophys. Res.* **104**, 14529–14541 (1999).
7. Parker, E. N. Sweet's mechanism for merging magnetic fields in conducting fluids. *J. Geophys. Res.* **62**, 509–520 (1957).
8. Sweet, P. A. *The Neutral Point Theory of Solar Flares* (Cambridge Univ. Press, 1958).
9. Xiao, C. J. *et al. In situ* evidence for the structure of a magnetic null in a 3D reconnection event in the Earth's magnetotail. *Nature Phys.* **2**, 478–483 (2006).
10. Gekelman, W. & Pfister, H. Experimental observations of the tearing of an electron current sheet. *Phys. Fluids* **31**, 2017–2025 (1988).
11. Linton, M. G. Dynamics of magnetic flux tubes in space and laboratory plasmas. *Phys. Plasmas* **13**, 058301 (2006).
12. Furno, I. *et al.* Current-driven rotating-kink mode in a plasma column with a non-line-tied free end. *Phys. Rev. Lett.* **97**, 015002–015004 (2006).
13. Sun, X., Intrator, T.P., Dorf, L., Furno, I. & Lapenta, G. Transition of MHD kink stability properties between line-tied and non line tied boundary conditions. *Phys. Rev. Lett.* **100**, 205004 (2008).
14. Haerendel, G., Paschmann, G., Sckopke, N. & Rosenbauer, H. The frontside boundary layer of the magnetosphere and the problem of reconnection. *J. Geophys. Res.* **83**, 3195–3216 (1978).
15. Roederer, J. G. Global problems in magnetospheric plasma physics and prospects for their solution. *Space Sci. Rev.* **21**, 23–71 (1977).
16. Phan, T. D. *et al.* A magnetic reconnection X-line extending more than 309 Earth radii in the solar wind. *Nature* **439**, 175–178 (2006).
17. Egedal, J. *et al.* Laboratory observations of spontaneous magnetic reconnection. *Phys. Rev. Lett.* **98**, 015003 (2007).
18. Baum, P. J. Plasma instability at an X-type magnetic neutral point. *Phys. Fluids* **16**, 1501–1504 (1973).
19. Frank, A. G. Magnetic reconnection and current sheet formation in 3D magnetic configurations. *Plasma Phys. Control Fusion* **41**, A687–A697 (1999).
20. Wan, W. & Lapenta, G. Micro–macro coupling in plasma self-organization processes during island coalescence. *Phys. Rev. Lett.* **100** 035004 (2008).
21. Biskamp, D. & Welter, H. Coalescence of magnetic islands. *Phys. Rev. Lett.* **44**, 1069–1071 (1980).
22. Knoll, D. A. & Chacon, L. Coalescence of magnetic islands in the low-resistivity, Hall-MHD regime. *Phys. Rev. Lett.* **96**, 135001–135004 (2006).
23. Furno, I. *et al.* Reconnection scaling experiment: A new device for three-dimensional magnetic reconnection studies. *Rev. Sci. Instrum.* **74**, 2324–2331 (2003).
24. Intrator, T. *et al.* Long lifetime current driven rotating kink modes in a non line-tied plasma column with a free end. *J. Geophys. Res.* **112**, A05S90 (2007).
25. Hemsing, E. W., Furno, I. & Intrator, T. P. Fast camera images of flux ropes during plasma relaxation. *IEEE Trans. Plasma Sci.* **33**, 448–449 (2005).
26. Intrator, T. P., Sun, X., Dorf, L., Furno, I. & Lapenta, G. A three dimensional probe positioner. *Rev. Sci. Instrum.* **79**, 10F129 (2008).
27. Ryutov, D. D., Furno, I., Intrator, T. P., Abbate, S. & Madziwa-Nussinov, T. Phenomenological theory of the kink instability in a slender plasma column. *Phys. Plasmas* **13**, 032105 (2006).
28. Lapenta, G., Furno, I., Intrator, T. & Delzanno, G. L. Kink instability of flux ropes anchored at one end and free at the other. *J. Geophys. Res.* **111**, A12S06 (2006).
29. Ji, H. *et al.* New insights into dissipation in the electron layer during magnetic reconnection. *Geophys. Res. Lett.* **35**, L13106 (2008).
30. Birn, J. & Priest, E. R. *Reconnection of Magnetic Fields* (Cambridge Univ. Press, 2007).
31. Hesse, M., Kuznetsova, M. & Birn, J. The role of electron heat flux in guide-field magnetic reconnection. *Phys. Plasmas* **11**, 5387–5397 (2004).
32. Anderson, C. & Priest, E. R. Time dependent magnetic annhilation at a stagnation point. *J. Geophys. Res.* **98**, 19395–19407 (1993).
33. Dorelli, J. C. & Birn, J. Whistler mediated magnetic reconnection in large systems: Magnetic flux pileup and the formation of thin current sheets. *J. Geophys. Res.* **108**, 1133 (2003).
34. Zweibel, E. G. & Rhoads, J. E. Magnetic merging in colliding flux tubes. *Astrophys. J.* **440**, 407–414 (1995).
35. Simakov, A. N., Chacon, L. & Knoll, D. A. Semi analytical model for flux pileup limited, dynamically reconnecting systems in resistive magnetohydrodynamics. *Phys. Plasmas* **13**, 082103 (2006).
36. Brackbill, J. U. FLIP MHD: A particle-in-cell method for magnetohydrodynamics. *J. Comput. Phys.* **96**, 163–192 (1991).
37. Milano, L. J., Dmitruk, P., Mandrini, C. H. & Gomez, D. O. Quasi separatrix layers in a reduced magnetohydrodynamic model of a coronal loop. *Astrophys. J.* **521**, 889–897 (1999).
38. Rogers, B. N., Denton, R. E., Drake, J. F. & Shay, M. A. Role of dispersive waves in collisionless magnetic reconnection. *Phys. Rev. Lett.* **87**, 195004 (2001).
39. Wang, Y., Kulsrud, R. & Ji, H. An analytic study of the perpendicularly propagating electromagnetic drift instabilities in the magnetic reconnection experiment. *Phys. Plasmas* **15**, 122105 (2008).
40. Mozer, F. S., Angelopoulos, V., Bonnell, J., Glassmeier, K. H. & McFadden, J. P. THEMIS observations of modified Hall fields in asymmetric magnetic field reconnection. *Geophys. Res. Lett.* **35**, L17S04 (2008).
41. Cramer, N, F. & Donnelly, I. J. Surface and discrete Alfvén waves in a current carrying plasma. *Plasma Phys. Control. Fusion* **26**, 1285–1298 (1984).

Acknowledgements

This work was supported by the Los Alamos Laboratory Directed Research and Development program under LANS Contract No. DE-AC52-06NA25396, and the Physics Frontier Center for Magnetic Self Organization in Laboratory and Astrophysical Plasmas, jointly funded by the National Science Foundation and the Department of Energy. We appreciate insightful comments from S. C. Hsu.

Author contributions

T.P.I. realized that our data showed 3D-instability-driven reconnection onset and stagnation and wrote this article, X.S. acquired most of the data and did substantial data analyses, G.L. carried out computational simulations of the RSX experiment, I.F. and L.D built much of the RSX experiment and discussed the results with T.P.I. and X.S. and solidified the arguments and presentation.

Additional information

Reprints and permissions information is available online at http://npg.nature.com/reprintsandpermissions. Correspondence and requests for materials should be addressed to T.P.I.